

# A spherical model with directional interactions: I. Static properties

Emanuela Zaccarelli,<sup>1</sup> Francesco Sciortino,<sup>1</sup> and Piero Tartaglia<sup>2</sup>

<sup>1</sup>*Dipartimento di Fisica and CNR-INFM-SOFT, Università di Roma La Sapienza, Piazzale A. Moro 2, I-00185, Rome, Italy*

<sup>2</sup>*Dipartimento di Fisica and CNR-INFM-SMC, Università di Roma La Sapienza, Piazzale A. Moro 2, I-00185, Rome, Italy*

(Dated: November 13, 2018)

We introduce a simple spherical model whose structural properties are similar to the ones generated by models with directional interactions, by employing a binary mixture of large and small hard spheres, with a square-well attraction acting only between particles of different size. The small particles provide the bonds between the large ones. With a proper choice of the interaction parameters, as well as of the relative concentration of the two species, it is possible to control the effective valence. Here we focus on a specific choice of the parameters which favors tetrahedral ordering and study the equilibrium static properties of the system in a large window of densities and temperatures. Upon lowering the temperature we observe a progressive increase in local order, accompanied by the formation of a four-coordinated network of bonds. Three different density regions are observed: at low density the system phase separates into a gas and a liquid phase; at intermediate densities a network of fully bonded particles develops; at high densities — due to the competition between excluded volume and attractive interactions — the system forms a defective network. The very same behavior has been previously observed in numerical studies of non-spherical models for molecular liquids, such as water, and in models of patchy colloidal particles. Differently from these models, theoretical treatments devised for spherical potentials, e.g. integral equations and ideal mode coupling theory for the glass transition can be applied in the present case, opening the way for a deeper understanding of the thermodynamic and dynamic behavior of low valence molecules and particles.

PACS numbers: 82.70.Gg, 82.70.Dd, 61.20.Lc

## I. INTRODUCTION

The study of dynamic arrest in atomic and molecular systems is an active field of research[1]. Close to the glass transition, in a small window of values of the external parameters (temperature or density/pressure) the dynamics of the system slows down by fifteen or more orders of magnitude. The slowing down of the dynamics varies in the temperature or density/pressure dependence from an Arrhenius law for the so-called strong network glass-forming liquids to a more complex super-Arrhenius behavior for fragile glass-forming liquids[2]. Signatures of the slowing down of the dynamics are observed at temperatures higher (or density lower) than the calorimetric glass transition and have been interpreted as the genuine precursor of the arrest phenomenon by the ideal Mode Coupling Theory (MCT)[3]. The study of the dynamics in colloidal systems[4, 5] has added new fuel to the discussion on dynamic arrest. Experimental realizations of simple models amenable to theoretical investigation has considerably boosted the understanding of the glass phenomenon and opened up an ampler view by adding to the arena the gelation issue, i.e. the possibility of observing arrest at low density, driven by the formation of inter-particle attractive bonds. Indeed, nowadays it is possible to realize colloidal systems which closely follow the hard-sphere (HS) equation of state, as well as to control an additional attractive interaction, both in range and in strength, moving the field of colloidal liquids towards molecular systems[6].

Recent studies have shown that when the hard-core is complemented by a spherical attractive potential, phase separation preempts the possibility of continuously approaching the slowing down of the dynamics at low density. For Lennard-Jones particles, Sastry[7] showed that the glass line intersects the liquid-gas spinodal on the liquid branch, suggesting that homogeneous arrested states are only possible for significantly large densities. More recently, the same scenario has been shown to hold even in the limit of very short-ranged spherical attractions[8, 9], down to the Baxter limit (infinitesimal attraction range). On the other hand, a series of studies have suggested that a progressive arrest at small packing fraction can be observed if the inter-particle interactions are highly directional (patchy interactions), when the effective valence becomes small[10]. On decreasing the valence below six, the gas-liquid unstable region progressively shrinks to smaller densities, opening up an intermediate region where a stable network of bonded particles forms. The shrinking of the unstable region can be tuned continuously down to a vanishing densities on decreasing the valence down to two[11]. When the average valence is slightly larger than two, it is possible to observe *empty liquids*, i.e. states with a temperature smaller than the critical temperature but with an extremely small liquid-state density. Numerical studies of the dynamics of liquids with patchy interactions have shown that the bond lifetime of the liquid network progressively increases upon cooling, providing evidence of the possibility of approaching arrested states continuously. The slowing down of the

arXiv:0708.0918v1 [cond-mat.dis-nn] 7 Aug 2007

dynamics in the newly accessible density region follows an Arrhenius law[12, 13, 14]. The arrest transition can be simultaneously interpreted in terms of *equilibrium gelation* in the colloid community[5, 12] and of *strong-glass* formation in the supercooled liquids community[13, 14]. These studies have clearly shown that reduction of valence is an essential ingredient for extending the glass line from the high-density/pressure region, dominated by repulsion, to intermediate regions where attraction and repulsion cooperate, down to the region of lower densities where attraction become the dominant arrest mechanism.

While simulations are a well documented method for studying the static and dynamic properties of non-spherical models, theoretical approaches are still not well developed, especially when the geometry of the bonds is such that inter-particle correlations propagate over several neighbors. The situation is even worse for microscopic theories of the glass transition, requiring structural quantities as input data. For the case of molecules, molecular[15, 16, 17, 18] and site-site[19, 20, 21] extensions of MCT have been developed, but their use has been limited due to the nature of the approximations and to the complexity of the calculations. An effective spherical approximation for non-spherical potentials has also been recently reported[22]. For these reasons, the theoretical evaluation of the MCT glass line for patchy non-spherical models has never been attempted so far. For the case of water (at ambient pressure) a molecular-MCT calculation has been reported[16, 23]. Besides water, the only network forming system whose slow dynamic properties have been investigated — starting from appropriate structural properties — is silica[24, 25, 26]. In the investigated model of silica, the network is formed by a binary mixture of two spherically interacting particles and hence all the complications associated to angular constraints are missing. Theoretical studies of silica have been limited to one specific value of the density and no clear picture of the glass-line in the  $T$ - $\rho$  plane has been provided.

As a first step toward a simple network-forming model for which theoretical calculations of the location of the arrest line in the phase diagram are in principle feasible, we introduce here a simple binary mixture model of particles interacting via short-range square well potentials and which is able to reproduce the same pattern (both for structural and dynamic quantities) of the previously studied non-spherical patchy models. The idea is borrowed from existing models for silica based on pair-wise additive interactions[27] but with a much simpler interaction potential. Due to the absence of the long-range electrostatic interactions, the model can be simulated in the entire phase diagram and the slowing down of the dynamics can be followed over a window of more than five orders of magnitude. The present article provides an evaluation of the structural properties of this model, based on extensive event-driven molecular dynamics simulations. A future companion article[28] will report the dynamic properties of the model. The manuscript is or-

ganized as follows: section II introduces the model; section III reports results for the structural, energetic and geometric properties. Section IV discusses the phase diagram, complemented by the study of various thermodynamic loci, while section V is devoted to conclusions.

## II. THE MODEL

Previously studied simple models for network forming liquids are based on many-body interactions[10, 29] or angular constraints[11, 30]. Here we introduce a simple model retaining both pair-wise additivity and spherical interactions, but which is capable of producing geometrical arrangement into a locally ordered network structure. The oxymoron spherical model with directional interactions is realised through the introduction of a second species in the mixture that represents a sort of floating bond. In this way, an effective one-component directional potential for the colloidal particles is obtained.

In more details, we consider  $N_1$  hard sphere colloids (for which we reserve the name *particles* in the following) with diameter  $\sigma_{11}$ . We mix them with  $N_2$  small particles with hard-sphere diameter  $\sigma_{22}$  (named *floating bonds* in the following). Particles and floating bonds interact via a non-additive (NA), short-ranged, attractive square-well (SW) potential of depth  $-u_0$  and range  $\delta$ . Thus, the floating bonds link particles providing a connection between them. More precisely the interaction potential is

$$\begin{aligned} V_{11}(r) &= \begin{cases} \infty & r < \sigma_{11} \\ 0 & r > \sigma_{11} \end{cases} \\ V_{12}(r) &= \begin{cases} \infty & r < \sigma_{12}^{NA} \\ -u_0 & \sigma_{12}^{NA} < r < \sigma_{12}^{NA} + \delta \\ 0 & r > \sigma_{12}^{NA} + \delta \end{cases} \\ V_{22}(r) &= \begin{cases} \infty & r < \sigma_{22} \\ 0 & r > \sigma_{22} \end{cases} \end{aligned} \quad (1)$$

We choose the potential parameters in such a way that (i) each floating bond binds no more than two particles; and (ii) the maximum number of floating bonds binding to a single particle is fixed, providing the valence of the model. To enforce condition (i), we recall that three identical touching hard-spheres of diameter  $\sigma_{11}$  create a cavity which can incorporate a hard-sphere with diameter up to  $d_c = (2/\sqrt{3} - 1)\sigma_{11} = 0.1547\sigma_{11}$  making contact with each of the three spheres. Hence, if the geometric condition  $\sigma_{12}^{NA} + \delta < (\sigma_{11} + d_c)/2$  is met, the floating bond can only be simultaneously involved in two attractive interactions. We choose  $\sigma_{12}^{NA} = 0.55\sigma_{11}$  and  $\delta = 0.03\sigma_{12}^{NA}$  so that  $2(\sigma_{12}^{NA} + \delta) - \sigma_{11} = 0.134\sigma_{11} < d_c$ . As a result of this choice, a floating bond can be isolated (with potential energy zero), bonded to one particle (potential energy  $-u_0$ ) or bonded to two distinct particles (potential energy  $-2u_0$ ). Only in the last case, the floating bond provides a link between the two particles, which

are thus considered bonded and belonging to the same cluster.

To satisfy the limited valence condition (ii) we fix the hard-sphere diameter of the floating bonds  $\sigma_{22}$ , determining the closest distance between them. To model a system with valence four (with tetrahedral ordering) we choose  $\sigma_{22} = 0.8\sigma_{11}$  (and hence, the mixture considered here has a negative non-additive parameter  $\Delta = \sigma_{12}^{NA}/(\sigma_{11} + \sigma_{22}) - 1 \simeq -0.69$ ). This choice is dictated by geometric considerations. Indeed, the distance between vertices of a perfect tetrahedron is  $2\sqrt{6}/3$  times the distance between the center and the vertex. The distance of an interacting floating bond from the center of a particle varies between  $\sigma_{12}^{NA}$  and  $\sigma_{12}^{NA} + \delta$ . Hence, a tetrahedral arrangement requires a value of  $\sigma_{22} < 0.93\sigma_{11}$ . To prevent the possibility of a planar square arrangement of bonds (a geometry which would allow a valence of six, with four bonds on the equatorial plane and two bonds on the poles) we need to impose  $\sigma_{22} > 0.802\sigma_{11}$ . We have checked that our choice  $\sigma_{22} = 0.8\sigma_{11}$  never generates particles connected to more than four floating bonds. Finally we fix the number ratio between particles and floating bonds following the stoichiometry of the system, i.e. by imposing that in the fully bonded ground state all particles participate to four bonds and that all floating bonds have energy  $-2u_0$ , i.e.  $N_2/N_1 = 2$ .

We study a system of  $N_1 = 1000$  particles and perform standard event-driven MD simulations in the NVE ensemble. For the smallest studied temperatures, equilibration requires several months of CPU time. Packing fraction is defined as  $\phi = \pi N_1(\sigma_{11}/L)^3/6$ , i.e. as the fraction of volume occupied only by the particles. In these units, taking into account the minimal and maximal bond distance between two particles, the diamond crystal is mechanically stable between  $0.233 < \phi < 0.255$  (since a diamond crystal of touching hard-spheres has  $\phi \simeq 0.340$ ). Units of length and energy are  $\sigma_{11}$  and  $u_0$ , while the Boltzmann constant  $k_B$  is set equal to 1. We equilibrated the mixture for a wide range of  $\phi$  and  $T$ , up to  $\phi = 0.56$  and down to  $T = 0.065$ . We notice that only for  $\phi \gtrsim 0.52$  crystallization (into a fcc structure) was sometimes (but not always) detected at low  $T$ .

The use of a square-well potential to model the interactions makes it possible to unambiguously define the existence of a bond between two large particle. Indeed, if the energy of a floating bonding particle is  $-2u_0$ , then the two large particles interacting with the floating bond particle are considered bonded. In this way, large particles can be partitioned into different clusters and the connectivity properties of them can be examined. More explicitly, to test for percolation, the simulation box is duplicated in all directions, and the ability of the largest cluster to span the replicated system is controlled. If the cluster in the simulation box does not connect with its copy in the duplicated system, then the configuration is assumed to be nonpercolating. The boundary between a percolating and a nonpercolating state point is then defined as the probability of observing infinite clusters in

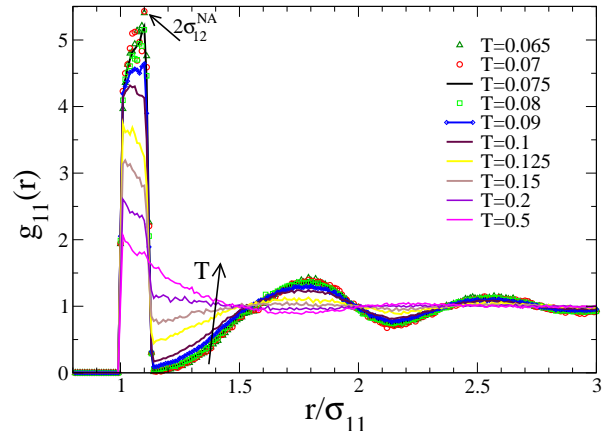


FIG. 1: Partial radial distribution function of particles  $g_{11}(r)$  along a low- $\phi$  isochore, i.e.  $\phi = 0.25$ , and upon decreasing  $T$ .

50% of the configurations.

### III. STATIC PROPERTIES

#### A. Radial distribution functions

To visualize how directional interactions build up for large particles upon decreasing temperature we report the behaviour of the particles radial distribution function  $g_{11}(r)$  in Fig. 1. At large  $T$ , no significant correlations are present and the system behaves almost as a hard-sphere fluid mixture. The first peak of  $g_{11}(r)$  is found at  $\sigma_{11}$ . However, as  $T$  is lowered, more and more particles are bonded within the attractive well, so that for  $\sigma_{11} < r < 2(\sigma_{12}^{NA} + \delta)$  a larger and larger correlation is built up. For  $r > 2(\sigma_{12}^{NA} + \delta)$  an anti-correlation develops. When  $T \lesssim 0.1$ , the peak of  $g_{11}(r)$  shifts from  $\sigma_{11}$  to  $2\sigma_{12}^{NA}$ , a signature of the progressive role played by the floating bonds in structuring the particles: while the growth at  $\sigma_{11}$  saturates, that at  $2\sigma_{12}^{NA}$  continues to increase.

A clear signal of the progressive structuring upon cooling is provided by the increase of the nearest neighbors peaks. The second peak is centered at a distance  $\approx 1.78\sigma_{11}$ , while the third one is found at  $\approx 2.53\sigma_{11}$ . Such a sequence of peak positions, with non-integer ratios, is typical of network-forming systems with tetrahedral arrangement[31, 32, 33]. It is also important to notice that, for  $T < 0.09$ , such peaks do not show a significant variation in intensity, indicating that the structuring process is essentially completed and that the system has approached an almost perfect long-range tetrahedral arrangement.

The density dependence of the partial radial distribution functions is reported, for  $T = 0.09$ , in Fig. 2. We first focus on the evolution of  $g_{11}(r)$  in the main panel.

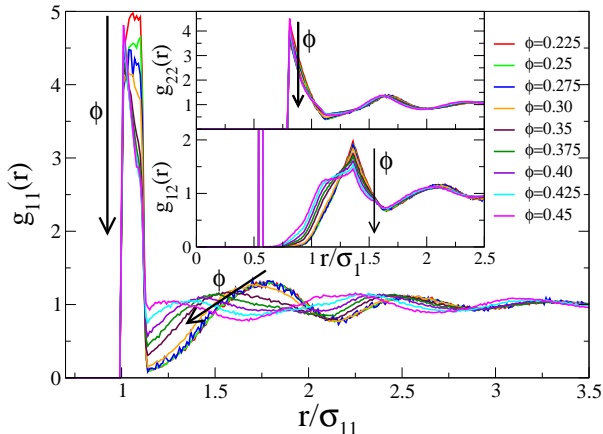


FIG. 2: Partial radial distribution functions of particles  $g_{11}(r)$  at fixed low  $T = 0.09$  and varying  $\phi$ . In the insets also partial radial distribution functions of floating bonds  $g_{22}(r)$  and of mixed type  $g_{12}(r)$  are shown.

Data show that the tetrahedral order, clearly visible at small and intermediate densities ( $0.225 < \phi < 0.40$ ), is progressively lost with increasing  $\phi$ . At this  $T$ , the curve corresponding to  $\phi = 0.30$  already shows small deviations in the location of the second peak. For larger  $\phi$  the location of the second peak moves to smaller distances and its amplitude decreases. Now the first peak is always found at  $\sigma_{11}$  rather than  $\sigma_{12}^{NA}$  for  $\phi \gtrsim 0.30$ . A similar shift and rearrangement is observed for secondary peaks, as well as for the evolution of the other partial distribution functions  $g_{12}(r)$  and  $g_{22}(r)$ , shown in the insets.

We further notice (not shown) that the  $\phi$ -value where tetrahedrality starts to get progressively lost is found to depend on  $T$ . On further decreasing  $T$ , the maximum  $\phi$  with dominant local order increases: at  $T = 0.08, 0.075$ , also  $\phi = 0.35$  becomes more tetrahedral-like. However, for  $\phi = 0.40$ , the structure even at the lowest equilibrated  $T$ , which is actually the closest point to the ground state structure that we could determine in our long-running simulations (see below), remains always far from that of a tetrahedral network.

These results suggest that geometric frustration due to packing acts against the formation of a tetrahedral network above a certain  $\phi$ , giving rise to a competition between energetic (directional attraction) and entropic (excluded volume) interactions.

### B. Static structure factor

We also study the behaviour of the normalized partial static structure factors, i.e.  $S_{ij}(q) = \langle |\rho_j(\mathbf{q})\rho_i(\mathbf{q})^*| \rangle / (N_i N_j)^{1/2}$ , where  $\rho_j(\mathbf{q}) = \sum_{m=1}^{N_j} \exp(i\mathbf{q} \cdot \mathbf{r}_m)$  is the wave vector  $\mathbf{q}$

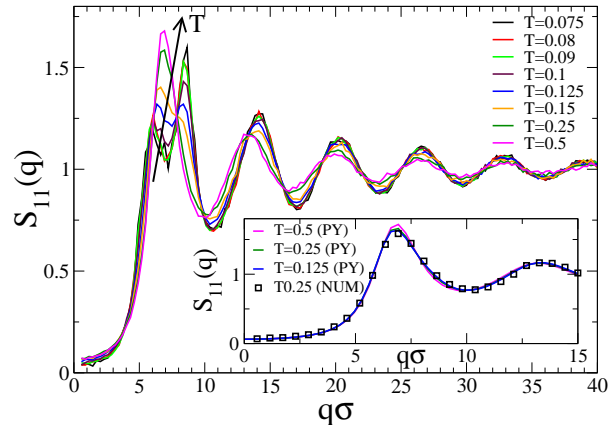


FIG. 3: Normalized  $S_{11}(q)$  for  $\phi = 0.35$  and varying  $T$ . Inset: Comparison with PY theoretical results.

component of the density of species  $j$  (and the sum runs over all  $N_j$  particles of type  $j$ ). We focus only on the partial structure factor of particles  $S_{11}(q)$ , aiming to emphasize those features that are characteristic of the establishment of a fully connected network of bonds. Figure 3 shows the behavior of  $S_{11}(q)$  as a function of  $T$  at  $\phi = 0.35$ . We notice that, at high  $T$ ,  $S_{11}(q)$  displays a nearest-neighbour peak centered around  $q\sigma \approx 7$ , characteristic of the hard-sphere interactions and of all simple liquids. As  $T$  is decreased the height of such a peak also decreases, eventually giving rise at low  $T$  to a splitting in two peaks: one for larger length-scales at  $q\sigma \sim 5$  and one at smaller length-scales  $q\sigma \sim 8.5$ . The first one seems to saturate at low  $T$ , while the second continues to increase in amplitude. The splitting of the main peak into two components is characteristic of network forming tetrahedral liquids [31, 34] and it is associated to the formation of an open local structure.

Simple integral equation theories are not able to predict the splitting of the peak on cooling. We solved numerically the binary Ornstein-Zernike equation for our mixture within Percus-Yevick (PY) approximation [35] at the same packing fraction  $\phi = 0.35$  upon lowering  $T$ . Results are shown in the inset of Fig. 3, together with a high- $T$  numerical curve. While at high  $T$  PY provides a good description of the system, it fails severely upon lowering  $T$ , where the splitting of the main peak is not at all captured. Moreover, numerical convergence of the PY solution can not be achieved for  $T < 0.125$ . Hence, the PY solution is only able to capture a small decrease of the peak, without accounting for the formation of the tetrahedral network, as expected due to the symmetric approximation contained in PY. This stresses the importance to develop more elaborated integral equations which are able to account for the angular correlations introduced by the bonding. In this respect, a step forward

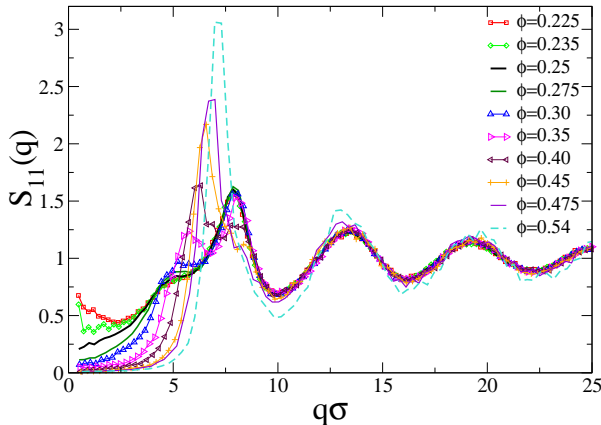


FIG. 4: Normalized  $S_{11}(q)$  for  $T = 0.09$  and varying  $\phi$ .

could be made by exploring PY approximation applied to the associative Ornstein-Zernike equation (PY-AOZ) which generally provides better results, compared to simulations, for network-forming liquids[36, 37].

The structure factor provides also information on the proximity to an unstable region since the low  $q$  behavior is related to the system compressibility. Indeed, close to an unstable state of the particles,  $S_{11}(q)$  increases significantly at small  $q$ . Figure 4 shows  $S_{11}(q)$  as a function of packing fraction, from  $\phi = 0.225$  (just close to the phase separation liquid boundary) to  $\phi = 0.54$  along a low temperature isotherm ( $T = 0.09$ ). On increasing  $\phi$ , the critical low  $q$  fluctuations disappear, giving rise to the network two-peak structure, then crossing continuously to a single-peaked standard  $S_{11}(q)$  that finally resembles that of high density simple liquids for  $\phi > 0.40$ .

The study of the structural properties reported so far clearly indicates that the possibility of forming a well-connected disordered tetrahedral network arises only in a finite window of intermediate densities, i.e.  $0.225 \lesssim \phi \lesssim 0.40$ . For smaller  $\phi$  values, particles are not close enough to form a fully bonded structure and phase separation into a gas and a bonded liquid is preferred. For larger values, the local density around each particle becomes more and more incompatible with the open structure which is characteristic of tetrahedral networks and packing becomes the leading driving mechanism controlling the structure.

### C. Energy

In the present model, attraction takes place only between particles and floating bonds. Moreover, the interaction range is such that each floating bond can interact simultaneously only with up to two distinct particles. This has the very important consequence that, for

the chosen  $N_1/N_2$  ratio, the energetic ground state of the system is known, being equal to two times the number of floating bonds (in units of  $-u_0$ ). In the present model, this means that a fully bonded configuration has a ground state energy  $E_{gs} = -2u_0N_2$  or equivalently  $E_{gs} = -4u_0N_1$ . We notice that an energetic gain is at hand both when a particle sticks to a floating bond (of contribution  $-u_0$ ) and when a true bond is established between two particles (of contribution  $-2u_0$ ). To differentiate between these two situations, we use  $E$  to indicate the potential energy of the system (i.e. proportional the number of connections between a particle and a floating bond), while we use  $E_b$  to count the potential energy associated to particle-particle bond contributions (i.e. proportional to the number of floating bonds with potential energy  $-2u_0$ ). Of course, the two quantities tend to become identical as  $T$  is lowered. We then define the bond probability as  $p_b \equiv (E_b - E_{gs})/E_{gs}$ .

The possibility of knowing theoretically the ground state of the system (a property shared with other limited valence models [11, 13, 14, 38, 39]) offers the possibility of unambiguously tracking the approach to the fully bonded state and detect the range of densities where indeed the system may reach continuously  $E_{gs}$ . It has been previously suggested [38] that the ability to reach in equilibrium almost fully bonded states is indeed a specific feature of network forming liquids.

Fig. 5(a) shows the potential energy relative to the ground state energy, expressed as  $E/E_{gs}$ , as a function of  $\phi$  for all studied temperatures. A magnification in semi-logarithmic scale of the low- $T$  isotherms is offered in Fig. 5(b) for the positive ratio  $(E - E_{gs})/E_{gs}$ . Except for high temperatures, for which the  $\phi$  dependence of  $E$  is monotonic (as in simple square-well models), a minimum in density appears. Since here the excluded volume interaction is modeled via a hard-core interaction, the increase of  $E$  at large  $\phi$  can arise only from a progressive breaking of the bonds. For intermediate  $T$ , when the average number of bonds per particle is still small, the minimum is met only at very large  $\phi$ . But, upon lowering  $T$ , bonding becomes more and more extensive and the density at the minimum progressively decreases, reaching  $\phi \approx 0.3$  at the lowest studied  $T$ . The  $T$ -dependence of the density minimum is shown in the phase diagram reported below (see Fig. 10).

Fig. 5(b) also shows that, in a large window of densities, the system is able to essentially reach the disordered ground state. Indeed, more than 95% of the bonds (intended as  $E_b$ ) are formed. This window of densities is roughly the same for which structural properties suggested the presence of a tetrahedral network of bonds. Since particles have already formed almost all possible bonds at the lowest studied temperatures, a further decrease in  $T$ , beyond the ones which we have been able to investigate, will not lead to further significant structural changes.

Being the ground state energy a priori known, it is possible to investigate the  $T$ -dependence of the energy



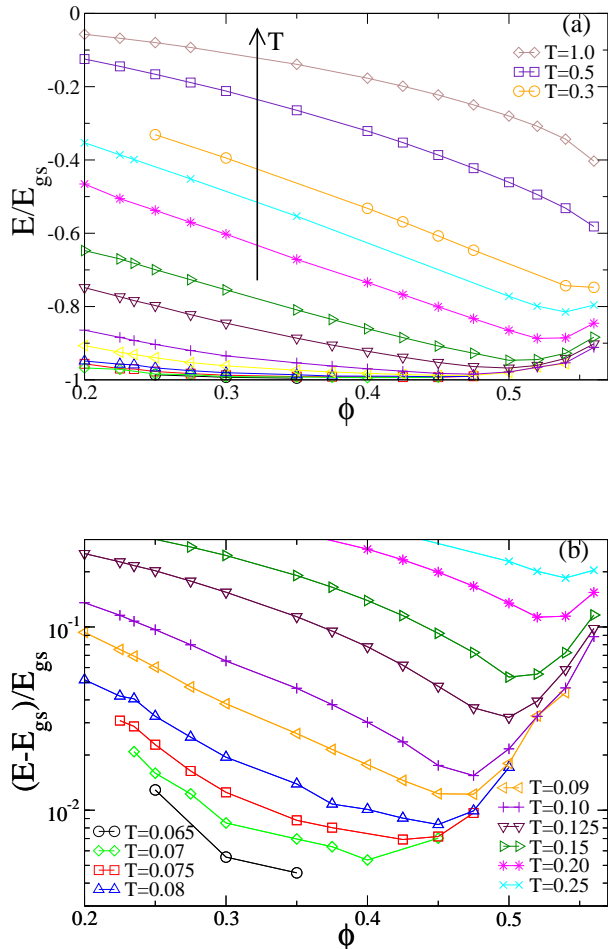


FIG. 5: Density dependence of the potential energy per particle relative to the ground state energy along different isochores: (a)  $E/E_{gs}$  for all studied state points and (b)  $(E - E_{gs})/E_{gs}$  in a magnification of the low  $T$  region in semi-logarithmic scale.

on approaching the fully bonded state. To this aim, Fig. 6 shows  $E - E_{gs}$  vs  $1/T$  in an Arrhenius plot for all investigated densities. Low  $\phi$  data are limited to the  $T$ -region above the liquid-gas instability. In the region where phase separation is not encountered, a clear Arrhenius dependence is found. However, for large enough densities, the energy decrease tends to saturate to a finite constant value. Only at intermediate densities ( $0.225 \lesssim \phi \lesssim 0.40$ ), it appears to be possible to reach a fully bonded (defect free) network. At larger densities the lowest energy state appears to be larger than the fully bonded one, suggesting that the total volume constraint imposes the presence of a finite number of defects in the fully bonded network. This is not surprising in view of the fact that the establishment of a tetrahedrally coordinated environment enforces a constraint on the local

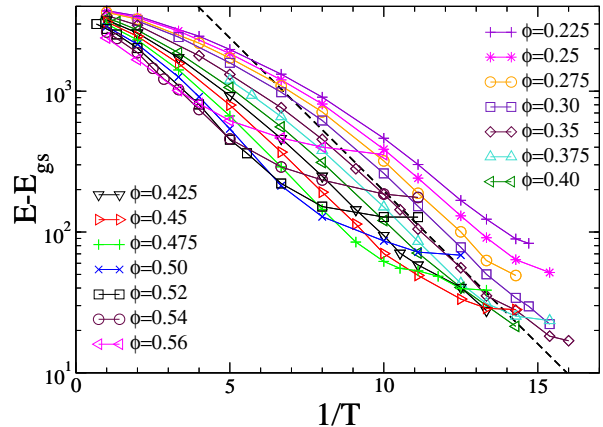


FIG. 6: Potential energy per particle  $E - E_{gs}$  vs.  $1/T$ . Note that at intermediate densities an Arrhenius approach to the ground state is observed. The dashed line is a reference curve with activation energy  $-0.5$ .

density.

To quantify the Arrhenius behaviour in an unbiased way, we fit the  $T$ -dependence of the potential energy with the functional form

$$[E - E_{gs}] = E_0 + B \exp(E_a/T) \quad (2)$$

in the region where a sufficient bonding is present. To realize this condition, we consider only state points where  $(E - E_{gs})/E_{gs} > 0.825$ , in order to have the same fitting conditions for all studied isochores. With the chosen fitting function, we can fully reproduce the behaviour of  $E$  both in the region where a fully connected network state is reached as well as that for states where frustration comes into play. Three fitting parameters are involved:  $E_0$ ,  $B$  and the activation energy  $E_a$ . The results of the fits are summarized in Fig. 7 for all studied  $\phi$ . We observe that the system approaches the expected ground state ( $E_0 = 0$ ) up to roughly  $\phi \sim 0.40$ , while a consistent increase of  $E_0$  is found at larger  $\phi$ . Hence, beyond such  $\phi$  value, the system can not reach a fully bonded configuration due to the excluded-volume contributions in the free energy. Even at vanishing temperatures, when minimization of the energy is the dominant driving force, it is impossible for geometric reasons to reach a fully bonded state and the effective ground state, reached along a constant  $\phi$  cooling path, is characterized by a non-zero fraction of unformed bonds. Data in Fig. 6 show that it is possible to unambiguously define an optimal region for network formation for  $0.235 \lesssim \phi \lesssim 0.40$  (the lower bound being fixed by the presence of phase separation). In this density window, the fully bonded ground state can be reached in equilibrium on isochoric cooling.

It is interesting to observe that the presence of a minimum in  $E(\phi)$  along isotherms is consistent with a defect-

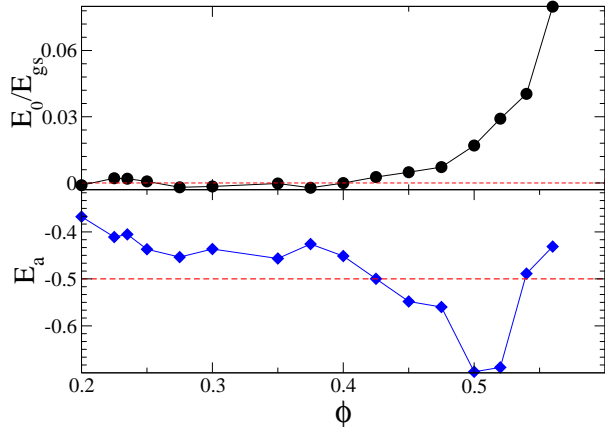


FIG. 7: Fit parameters from the fitting Arrhenius law in Eq. 2: effective ground-state energy ratio  $E_0/E_{gs}$  (top) and activation energy  $E_a$  (bottom).

free ground state, but only in a small region of densities. The optimal network-forming region largely coincides with that where the structural properties also show tetrahedral arrangement, with the exception of the state points close to  $\phi = 0.40$ , where still  $E_0 \rightarrow 0$  even though the network begins to be deformed due to the increase in packing. Such feature is only possible in the present model due to the flexibility of the chosen interaction parameters.

The  $\phi$ -dependence of the activation energy (bottom panel) is also instructive. It is observed that  $E_a$  is slightly larger than  $-0.5$  within the optimal network-forming region, showing an almost monotonic decrease up to  $\phi \sim 0.50$ , then a reversal of trend is observed at the highest studied values. Note that the value 0.5 is the theoretical value expected for the breaking process of independent bonds[40].

The low  $T$  Arrhenius behavior carries with it another important thermodynamic feature, the presence of a maximum in the constant volume  $V$  specific heat  $C_V$ . The behaviour of  $C_V$  along the studied isochores is reported in Fig. 8. In this respect, the present model confirms the suggestion[39] that a line of  $C_V$  maxima in the phase diagram is present when bonding is the relevant driving force. Differently from the model in Ref. [39], a monotonic increase of the  $T$ -value of the  $C_V$ -maxima is observed upon increasing  $\phi$ . It is not a coincidence that maxima in  $C_V$  are also characteristic of reversible self-assembly processes[41, 42], i.e. of systems in which bonding plays the leading role. The locus of  $C_V$ -maxima extracted from these results will be discussed in Sec. IV.

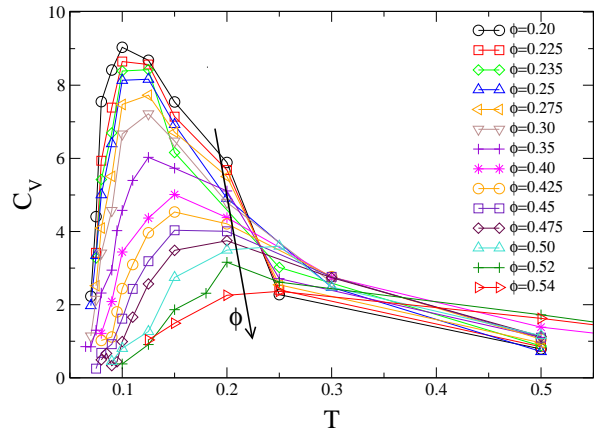


FIG. 8: Constant volume specific heat  $C_V = (dE/dT)_V$  for all studied isochores.

#### D. Angular distribution of bonds

A direct measure of the tetrahedral structure of the network is offered by the evaluation of the distribution of the angle  $\theta$  between bonded triplets of large particles, repeating the analysis that is usually performed for similar models[43, 44, 45]. The angle distribution  $P(\theta)$  is shown as a function of  $\phi$  for  $T = 0.075$  in Fig. 9(a). For  $\phi \lesssim 0.30$ ,  $P(\theta)$  is almost independent of  $\phi$ , suggesting the approach to a tetrahedral network with almost fully connected particles. A peak close to the tetrahedral angle is found, and an average value of the triplet angle of  $\approx 108.2$ . Also, around  $\theta = 0.60$  a secondary peak is observed, a geometric signature of the presence of a small number of three-particle rings[43, 45]. A Gaussian fit is attempted (dashed curve in Fig. 9(a)), which works well only in the large- $\theta$  region, due to the presence of rings. In agreement with the structural indicators discussed previously,  $P(\theta)$  deviates more and more from the typical tetrahedral shape on increasing  $\phi$ . When the excluded volume contribution becomes dominant over the attractive interactions, the main tetrahedral peak is progressively lost and a wider distribution is observed, accompanied also by a smaller average angle and by an increase of three-particles loops.

In Fig. 9(b) a comparison of  $P(\theta)$  for different 4-coordinated models is offered, completing the data already presented in [14]. In that work,  $P(\theta)$  for a model without any geometric correlation in the location of the bonding sites (the  $N_{max}$  model[12, 46, 47]) — showing a rather flat distribution of angles due to the lack of preferred orientation between the bonds (i.e. random bond organization) — was compared with  $P(\theta)$  for two models with well defined locations of the bonding sites on the particles surface, the so-called primitive models of water (PMW)[48] and primitive models of silica (PMS)[49].

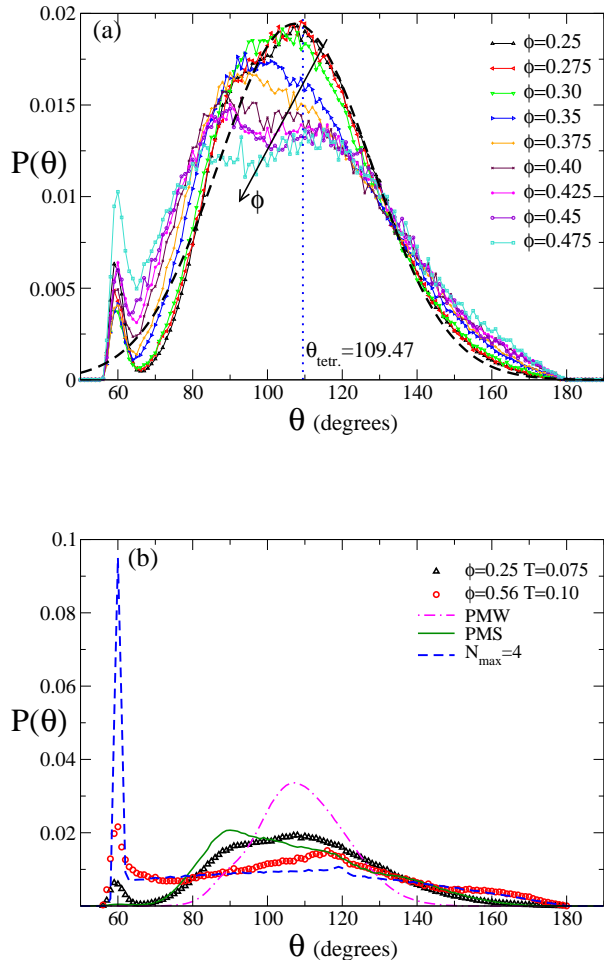


FIG. 9: Distribution of the angle  $\theta$  between bonded particles triplets. Full thin lines are guides to the eye. (a)  $P(\theta)$  for various  $\phi$  at  $T = 0.075$ . The thick dashed line is a Gaussian fit to the low- $\phi$  states, suggesting an average angle  $\sim 107.4$  and variance  $\sim 29.0$ ; (b) Comparison of  $P(\theta)$  in the optimal network-forming density ( $\phi = 0.25, T = 0.075$ —triangles) with different 4-coordinated models: PMW (dot-dashed line), PMS (full line),  $N_{max}$  (dashed line) (all from Ref. [14]), as well as for the present model at two different state points (triangles and circles).

The PMW, at its optimal density, displays a quite sharp and narrow peak, with an average angle  $\simeq 109$  degrees, due to the rigid organization of the bonding sites modeling the hydrogen atoms and the lone-pairs of the water molecule, with a roughly Gaussian shape of  $P(\theta)$ . On the other hand, the PMS at its optimal network-forming density has a wider and more asymmetric distribution, which is peaked at lower angles  $\theta \approx 90$  degrees. In addition, the  $N_{max}$  model was found to exhibit a dominant contribution of three-particles loops or touching triplets ( $\theta = 60$  degrees), a feature that was absent in PMW and negligible in PMS. Comparing the results for the present binary

model to the existing data, we observe that, within the optimal network-forming region, the organization of particles is very reminiscent of that of PMS, except for a shift of the peak position, which is closer to the tetrahedral position, as well as for a more pronounced presence of loops. Interestingly, when  $\phi$  is increased, local tetrahedral order is lost, as for the reported  $\phi = 0.56$ -curve, and  $P(\theta)$  tends to the  $N_{max}$  distribution, confirming that the organization of the bonds becomes increasingly random.

### E. Liquid-Gas unstable region

Although we do not perform accurate phase coexistence studies, we can provide a rough estimate of the location of the liquid-gas phase separation region and of the associated critical point by a combined check of the time evolution of the large length-scale structural properties, such as  $S(q \rightarrow 0)$ , as well as of the pressure behaviour along different isotherms. The lowest investigated  $\phi$  where phase separation can be ruled out at all studied temperatures is  $\phi = 0.25$ . For lower  $\phi$ , we detect an increase of  $S(q \rightarrow 0)$  as well as the development of maxima and minima in the behaviour of  $P(\phi)$  (coming respectively from small and large  $\phi$ ). We define, for each  $T$ , the location in  $\phi$  of such maxima and minima as the spinodal points. We note that at  $T = 0.1$  the pressure dependence on  $\phi$  does not show any loop, while at  $T = 0.095$  a small instability region seems to be present (within our numerical resolution) close to  $\phi \sim 0.10$ . These two temperatures thus bracket the critical temperature  $T_c$ . Hence, we estimate  $T_c = 0.095 \pm 0.005$ , while  $\phi_c = 0.10 \pm 0.025$ . A more accurate evaluation of the critical parameters, with appropriate techniques should be undertaken in future studies. We also note that the value of  $\phi$  at which no critical fluctuations are observed in the entire investigated  $T$ -range is in close agreement both with the  $N_{max}$  model[10] with coordination number four as well as with the PMW[13] and PMS[14] models, reinforcing the view that the valency is the control parameter for the location of the liquid-gas spinodal[11], under single-bond conditions.

## IV. A GLOBAL LOOK AT THE PHASE DIAGRAM

To summarize the static properties and to provide a coherent picture of the system behaviour, we discuss here the phase diagram of the model, in combination with other relevant thermodynamic and connectivity loci.

Fig. 10 shows the liquid-gas spinodal, the locus encompassing the region of thermodynamic instability. It is worth emphasizing that such instability region is confined to densities much smaller than those observed in spherical attractive potentials. Liquid densities are roughly half of the typical value of normal liquids, highlighting the large empty spaces which characterize the formation



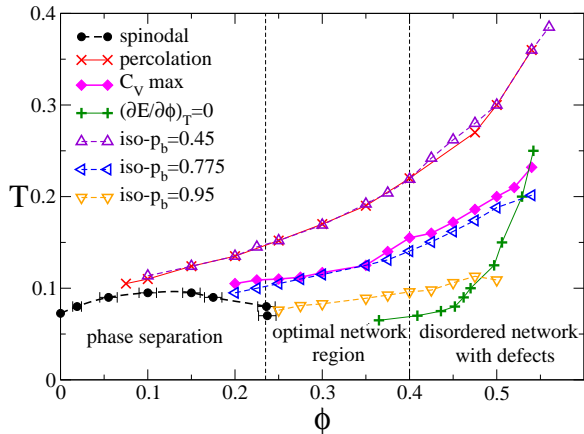


FIG. 10: Static phase diagram in the  $(\phi, T)$  plane of the studied spherical binary model. The reported lines are: gas-liquid spinodal (circles), percolation line (x-symbols), locus of  $C_V$  maxima (diamonds), iso- $p_b$  lines at selected values (triangles) and energy minima (crosses). Lines are guides to the eye. Vertical dashed lines show the liquid boundary of the spinodal line ( $\phi \sim 0.235$ ) and the boundary ( $\phi \sim 0.40$ ) between the optimal network region, where bonds are primarily directional, and that of a disordered network with defects, where directionality is progressively lost.

of a tetrahedral network. At the same time, the small- $\phi$  location of the liquid branch of the spinodal shows that, in this model, it is possible to find a region of intermediate densities where, on lowering  $T$ , the system remains homogeneous down to very small  $T$ , a feature which is not possible with spherically symmetric attractive potentials. Moreover, the liquid branch of the spinodal terminates in a region which is compatible with the window of stability of the diamond crystal[50, 51]. This topology of the liquid-gas coexistence is typical of models with directional interactions, and it is here confirmed through the use of our spherical binary mixture.

To provide an indication of the degree of bonding observed in different regions of the phase diagram, Fig. 10 also shows constant bond-probability lines (iso- $p_b$  lines), i.e. lines of constant number of bonds per particles. Here a bond is defined as a floating bond with potential energy  $-2u_0$ . The lines have positive slope, signaling that on increasing density bond formation becomes favored. Only at very large  $\phi$  and very large  $p_b$  (only visible for  $p_b = 0.95$  in the figure for the highest density point), a sharp change of slope (flat, then negative at even larger  $p_b$ ) is found, associated to the disruptive effect of increasing density beyond the values for optimal network formation.

Fig. 10 also shows the percolation line and the locus of  $C_V$  maxima. State points on the right-hand side of the percolation line are characterized by the presence of an infinite cluster in  $> 50\%$  of the configurations. This

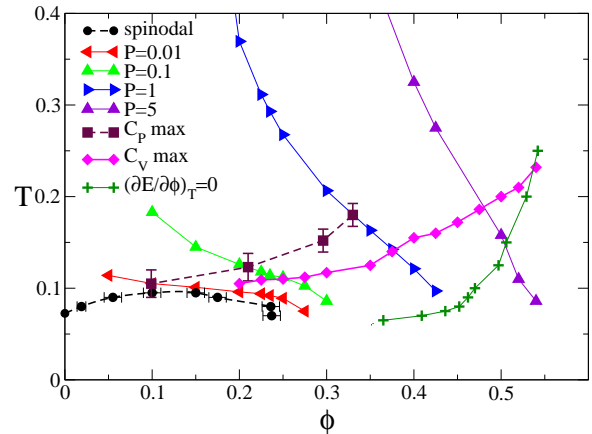


FIG. 11: Static phase diagram in the  $(\phi, T)$  plane of the studied spherical binary model. In addition to lines reported in Fig. 10, i.e. gas-liquid spinodal (circles), locus of  $C_V$  maxima (diamonds) and of energy minima (crosses), several isobaric paths are shown (triangles). Moreover, the locus of  $C_P$  maxima (squares) is also reported, merging into the spinodal line at the critical point.

definition of percolation locus is strictly a geometric measure and does not provide any information on the lifetime of the spanning cluster[5]. The percolation locus coincides, within numerical resolution, with the  $p_b = 0.45$  locus, suggesting that a constant fraction of bonds is requested to percolate independently of  $\phi$ . The  $p_b$  value at percolation,  $p_b^{perc} \sim 0.45$ , is slightly larger than the one for random bond percolation on a diamond lattice, known to be  $p_b = 0.388$ [52], an effect which can be attributed to the disordered distribution of particles in the fluid. The percolation locus is located above the critical point, confirming that the development of long range correlated critical fluctuations requires as a prerequisite the existence of a spanning network of bonded particles[53]. The locus of  $C_V$  maxima is located well inside the percolation region and, by comparing with the iso- $p_b$  curves, it takes place when the bond probability is  $\approx 0.75$ . Comparing with published data of models with different valency[39, 41, 42] it appears that the  $C_V$  maxima line progressively moves to larger and larger  $p_b$  values with increasing valence. The trend is thus opposite to the one characterizing the valence dependence of  $p_b^{perc}$ . Finally, Fig. 10 also shows the locus of potential energy minima along isotherms, i.e. for which  $(\partial E/\partial\phi)_T = 0$ , a line marking the crossover from an unconstrained network of bonds to a state in which bonding can not be any longer optimized due to volume constraints.

Additional information on the  $T$  and  $\rho$  dependence of the properties of the model are reported in Fig. 11. This shows, in addition to some of the lines reported in the previous figure, the location of selected isobars with the pressure  $P$  varying by more than two orders of magni-

ude. From the constant- $P$  paths, we evaluate the enthalpy  $H = E + PV$ , and we extract the behaviour of the constant-pressure specific heat  $C_P = (\partial H/\partial T)_P$ . We find the presence of clear maxima also in  $C_P$ , whose locus is also reported in Fig. 11. The line of  $C_P$  maxima is an example of a Widom line[54, 55], which starts, by definition, from the critical point. Its calculation therefore also confirms the previously discussed estimate of the critical point within our numerical resolution. Finally we observe that, in the investigated  $T$  region, there is no evidence of anomalies in the density (constant  $P$  density maxima), that are commonly found in water models[13, 56, 57].

## V. CONCLUSIONS

In this article we have introduced an opportunely designed, spherical binary mixture model, which is able to generate a fluid with a effective coordination number of four. Differently from previously studied four-coordinate model[10, 11, 12, 13, 14], the particle-particle interactions are spherical, a feature which is important in order to allow a future comparison with theoretical approaches.

We have shown that the static phase diagram of the system is very similar to the one reported for patchy models[12, 13, 14, 58], as well as for more sophisticated models of network forming liquids[27, 56]. Indeed, the unstable phase-separating region of the system is confined to low packing fraction  $\phi$  and small  $T$ , consistently with previous studies and Wertheim theory calculations [11] for four-coordinated particles. This reinforces the statement, that, from the point of view of suppressing phase separation, the arrangement of the sticky points onto the particle surface is not qualitatively, but only quantitatively relevant.

The unstable gas-liquid region is followed at larger densities by an optimal network region, i.e. a window of densities where the system can be equilibrated down to very low temperatures observing a progressive formation of a tetrahedral network of bonds. In this region, the system almost reaches the fully bonded configuration, i.e. the disordered ground state of the system and hence a fur-

ther lowering of the temperature would not produce any significant structural change. For even larger densities, we observe a destruction of the tetrahedral bonding, induced by the packing constraints. A signature of this effect is observed in both the structure factor of the system, which crosses from the tetrahedral-network form to the hard-sphere form as well as in the progressive breaking of the bonds on isothermal increase of the density.

It is also interesting to discuss the relative location of the percolation locus, the locus of specific heat maxima and the liquid-gas spinodal. In the present model, the percolation line provides the first indication of the clustering process upon lowering  $T$ . Successive cooling brings to the presence of a line of  $C_V$  maxima, and finally of the spinodal line. The constant-volume specific heat maxima line appears to be a characteristic of all bonded systems, since it is observed also in the case of valence two[41] where no percolation is present. Its relative location has an opposite dependence on the bond probability as compared to the percolation line, when studied as a function of the valence. This suggests that, for values of the valence larger than the one studied here, the line of  $C_V$  maxima may become buried in the region where equilibration is not feasible any longer, i.e. in the glass state. This could be the reason why it is not observed in standard spherical models, such as a simple square-well potential.

Finally, we note that the possibility of generating the complex pattern characteristic of tetrahedral liquids with a simple binary mixture with pair-wise additive square-well interactions opens the possibility of applying the tools of modern liquid theory (which are nowadays particularly accurate for spherical potentials) to the present case. It will also be possible, using theoretical and/or numerical structure factors investigate the dynamics of the present system using the formalism of the Mode Coupling Theory for the glass transition. Work in this direction is underway and a companion paper on the dynamics will appear shortly.

We acknowledge support from MIUR Prin and MRTN-CT-2003-504712. We thank C. N. Likos and I. Saika-Voivod for useful discussions.

- 
- [1] K. Binder and W. Kob, *Glassy Materials and Disordered Solids: An Introduction to their Statistical Mechanics* (World Scientific, 2005).
  - [2] C. A. Angell, *J. Non-Cryst. Solids* **73**, 1 (1985).
  - [3] W. Götze, *Liquids, Freezing and the Glass Transition* (North-Holland Amsterdam, 1991), pp. 287–503.
  - [4] F. Sciortino and P. Tartaglia, *Advances in Physics* **54**, 471 (2005).
  - [5] E. Zaccarelli, *J. Phys.: Condens. Matter* **19**, 323101 (2007).
  - [6] T. Voigtmann and W. C. K. Poon, *J. Phys.: Condens. Matter* **18**, L465 (2006).
  - [7] S. Sastry, *Phys. Rev. Lett.* **85**, 590 (2000).
  - [8] E. Zaccarelli, F. Sciortino, S. V. Buldyrev, and P. Tartaglia, *Short-ranged attractive colloids: What is the gel state?* (Elsevier, Amsterdam, 2004), pp. 181–194.
  - [9] G. Foffi, C. De Michele, F. Sciortino, and P. Tartaglia, *Phys. Rev. Lett.* **94**, 078301 (2005).
  - [10] E. Zaccarelli, S. V. Buldyrev, E. La Nave, A. J. Moreno, I. Saika-Voivod, F. Sciortino, and P. Tartaglia, *Phys. Rev. Lett.* **94**, 218301 (2005).
  - [11] E. Bianchi, J. Largo, P. Tartaglia, E. Zaccarelli, and F. Sciortino, *Phys. Rev. Lett.* **97**, 168301 (2006).
  - [12] E. Zaccarelli, I. Saika-Voivod, A. J. Moreno, S. V. Buldyrev, P. Tartaglia, and F. Sciortino, *J. Chem. Phys.* **124**, 124908 (2006).

- [13] C. De Michele, S. Gabrielli, P. Tartaglia, and F. Sciortino, *J. Phys. Chem. B* **110**, 8064 (2006).
- [14] C. De Michele, P. Tartaglia, and F. Sciortino, *J. Chem. Phys.* **125**, 4710 (2006).
- [15] R. Schilling and T. Scheidsteger, *Phys. Rev. E* **56**, 2932 (1997).
- [16] L. Fabbian, A. Latz, R. Schilling, F. Sciortino, P. Tartaglia, and C. Theis, *Phys. Rev. E* **60**, 5768 (1999).
- [17] R. Schilling, *J. Phys.: Condens. Matter* **12**, 6311 (2000).
- [18] C. Theis, F. Sciortino, A. Latz, R. Schilling, and P. Tartaglia, *Phys. Rev. E* **62**, 1856 (2000).
- [19] S. H. Chong and F. Hirata, *Phys. Rev. E* **58**, 6188 (1998).
- [20] S. H. Chong and F. Sciortino, *Phys. Rev. E* **69**, 051202 (2004).
- [21] S.-H. Chong and W. Götze, *Phys. Rev. E* **65**, 041503 (2002).
- [22] G. Yatsenko and K. S. Schweizer, *J. Chem. Phys.* **126**, 4505 (2007).
- [23] L. Fabbian, A. Latz, R. Schilling, F. Sciortino, P. Tartaglia, and C. Theis, *Phys. Rev. E* **62**, 2388 (2000).
- [24] F. Sciortino and W. Kob, *Phys. Rev. Lett.* **86**, 648 (2001).
- [25] B. Coluzzi and P. Verrocchio, *J. Chem. Phys.* **116**, 3789 (2002).
- [26] W. Kob, M. Nauroth, and F. Sciortino, *J. Non-Cryst. Sol.* **307**, 181 (2002).
- [27] B. W. H. van Beest, G. J. Kramer, and R. A. van Santen, *Phys. Rev. Lett.* **64**, 1955 (1990).
- [28] E. Zaccarelli, F. Sciortino, and P. Tartaglia, in *preparation* (2007).
- [29] J. Largo, P. Tartaglia, and F. Sciortino, *Phys. Rev. E* **76**, 011402 (2007).
- [30] N. Kern and D. Frenkel, *J. Chem. Phys.* **118**, 9882 (2003).
- [31] J. Horbach and W. Kob, *Phys. Rev. B* **60**, 3169 (1999).
- [32] N. Giovambattista, H. E. Stanley, and F. Sciortino, *Phys. Rev. E* **72**, 031510 (2005).
- [33] T. Loerting and N. Giovambattista, *J. Phys.: Condens. Matter* **18**, 919 (2006).
- [34] F. W. Starr, M.-C. Bellissent-Funel, and H. E. Stanley, *Phys. Rev. E* **60**, 1084 (1999).
- [35] J. P. Hansen and I. R. MacDonald, *Theory of Simple Liquids* (Academic, London, 2006), 3rd ed.
- [36] Y. Duda, C. J. Segura, E. Vakarin, M. F. Holovko, and W. G. Chapman, *J. Chem. Phys.* **108**, 9168 (1998).
- [37] Y. Duda, *J. Chem. Phys.* **109**, 9015 (1998).
- [38] A. J. Moreno, S. V. Buldyrev, E. La Nave, I. Saika-Voivod, F. Sciortino, P. Tartaglia, and E. Zaccarelli, *Phys. Rev. Lett.* **95**, 157802 (2005).
- [39] A. J. Moreno, I. Saika-Voivod, E. Zaccarelli, E. L. Nave, S. V. Buldyrev, P. Tartaglia, and F. Sciortino, *J. Chem. Phys.* **124**, 204509 (2006).
- [40] M. Wertheim, *J. Stat. Phys.* **35**, 19 (1984), ; 1984 *J. Stat. Phys.* **35** 35; 1986 *J. Chem. Phys.* **85** 2929.
- [41] F. Sciortino, E. Bianchi, J. Douglas, and P. Tartaglia, *J. Chem. Phys.* **126**, 194903 (2007).
- [42] E. Bianchi, E. La Nave, P. Tartaglia, and F. Sciortino (2007).
- [43] J. P. Rino, I. Ebbsjö, R. K. Kalia, A. Nakano, and P. Vashishta, *Phys. Rev. B* **47**, 3053 (1993).
- [44] N. Mousseau and L. J. Lewis, *Phys. Rev. Lett.* **78**, 1484 (1997).
- [45] K. Vollmayr, W. Kob, and K. Binder, *Phys. Rev. B* **54**, 15808 (1996).
- [46] R. J. Speedy and P. G. Debenedetti, *Mol. Phys.* **81**, 237 (1994).
- [47] R. J. Speedy and P. G. Debenedetti, *Mol. Phys.* **88**, 1293 (1996).
- [48] J. Kolafa and I. Nezbeda, *Mol. Phys.* **61**, 161 (1987).
- [49] M. H. Ford, S. M. Auerbach, and P. A. Monson, *J. Chem. Phys.* **121**, 8415 (2004).
- [50] F. Romano, P. Tartaglia, and F. Sciortino, *J. Phys.: Condens. Matter* **19**, F2101+ (2007).
- [51] C. Vega and P. A. Monson, *J. Chem. Phys.* **109**, 9938 (1998).
- [52] D. Stauffer and A. Aharony, *Introduction to Percolation Theory* (Taylor and Francis, London, 1992), 2nd ed.
- [53] A. Coniglio and W. Klein, *J. Phys. A* **13**, 2775 (1980).
- [54] L. Xu, P. Kumar, S. V. Buldyrev, S.-H. Chen, P. H. Poole, F. Sciortino, and H. E. Stanley, *Proc. Nat. Ac. Sci.* **102**, 16558 (2005).
- [55] P. Kumar, S. V. Buldyrev, S. R. Becker, P. H. Poole, F. Starr, and H. E. Stanley, *Proc. Nat. Ac. Sci.* **104**, 9575 (2007).
- [56] P. H. Poole, I. Saika-Voivod, and F. Sciortino, *J. Phys.: Condens. Matter* **17**, L431 (2005).
- [57] P. H. Poole, F. Sciortino, U. Essmann, and H. E. Stanley, *Nature* **360**, 324 (1992).
- [58] J. Largo, F. W. Starr, and F. Sciortino, *Langmuir* **23**, 5896 (2007).